Influence of Disorder and Anharmonic Fluctuations on the Dynamical Rashba Effect in Purely Inorganic Lead-Halide Perovskites

Arthur Marronnier, Guido Roma, Marcelo Carignano, Yvan Bonnassieux, Claudine Katan, Jacky Even, Edoardo Mosconi, Filippo de Angelis

Influence of Disorder and Anharmonic Fluctuations on the Dynamical Rashba Effect in Purely Inorganic Lead-Halide Perovskites

Arthur Marronnier,[†] Guido Roma,[*,‡] Marcelo Carignano,[¶] Yvan Bonnassieux,[†] Claudine Katan,[§] Jacky Even,[‖] Edoardo Mosconi,[⊥] and Filippo De Angelis[⊥,#]

[†]*LPICM, CNRS, Ecole Polytechnique, Université Paris-Saclay, 91128 Palaiseau, France*

[‡]*DEN - Service de Recherches de Métallurgie Physique, CEA, Université Paris-Saclay, 91191 Gif sur Yvette, France*

[¶]*Qatar Environment and Energy Research Institute, Hamad Bin Khalifa University, P.O. Box 5825, Doha, Qatar*

[§]*Univ Rennes, ENSCR, INSA Rennes, CNRS, ISCR (Institut des Sciences Chimiques de Rennes) – UMR 6226, F-35000 Rennes, France*

[‖]*Univ Rennes, INSA Rennes, CNRS, Institut FOTON — UMR 6082, F-35000 Rennes, France*

[⊥]*Computational Laboratory for Hybrid/Organic Photovoltaics (CLHYO), CNR-ISTM, Via Elce di Sotto 8, I-06123 Perugia, Italy*

[#]*D3-CompuNet, Istituto Italiano di Tecnologia, Via Morego 30, 16163 Genova, Italy*

E-mail: guido.roma@cea.fr

Abstract

Doping organic metal-halide perovskites with cesium could be the best solution to stabilize highly-efficient perovskite solar cells. The understanding of the respective roles of the organic molecule, on one hand, and the inorganic lattice, on the other, is thus crucial in order to be able to optimize the physical properties of the mixed-cation structures. In particular, the study of the recombination mechanisms is thought to be one of the key challenges towards full comprehension of their working principles. Using molecular dynamics and frozen phonons, we evidence sub-picosecond anharmonic fluctuations in the fully inorganic $CsPbI_3$ perovskite. We reveal the effect of these fluctuations, combined with spin-orbit coupling, on the electronic band structure, evidencing a dynamical Rashba effect. Our study shows that under certain conditions space disorder can quench the Rashba effect. As for time disorder, we evidence a dynamical Rashba effect which is similar to what was found for $MAPbI_3$ and which is still sizable despite temperature disorder, the large investigated supercell, and the absence of the organic cations' motion. We show that the spin texture associated to the Rashba splitting cannot be deemed responsible for a consistent reduction of recombination rates, although the spin mismatch between valence and conduction band increases with the ferroelectric distortion causing the Rashba splitting.

Introduction

Fully inorganic metal-halide perovskites have attracted more and more attention in the past two years as they have showed promising efficiencies (record efficiency of 13.4% for quantum dot devices[1] and of 15.07% recently reported for a thin film[2]) and as cesium doping has proven to be a good way to improve the environmental stability of hybrid metal-halide perovskites.[3] Moreover, a better understanding of the physical properties of fully inorganic halide perovskites is needed in order to further understand, by contrast, the role of the organic cation in their hybrid cousins.

In general, the enthusiasm for metal-halide perovskites can be explained by their exceptional optoelectronic properties, whether it be their optical properties,[4–7] the long lifetimes of both electrons and holes[8–10] and the high mobility in these materials.[10,11] Another remarkable feature of these materials is the fact that they present good absorption and charge generation properties,[12,13] but to fully exploit this for solar cells one should be able to control all the factors that limit overall recombination rates. If the former —absorption— could be explained in particular by the materials' direct band gap, for the latter —recombination— one expects high values for both the radiative (direct band gap) and non-radiative recombination (high density of defects). As for defects, one should note that charge separation could be actually eased in these materials through halide ionic migration[14,15] which could either favour exciton screening[16] or give birth to local screening domains.[17,18]

Concerning radiative recombination, which has been indeed shown to be relatively high,[19] one should take into account the interplay of spin and orbital degrees of freedom, which is considerable in these materials because of the presence of the heavy lead atoms. In particular, the giant spin-orbit coupling (SOC) that was reported in these materials[20] is expected to be at the origin of Rashba-like splittings.[21–24] Such splittings correspond to the lift of the electronic bands' spin degeneracy in the presence of SOC and time reversal symmetry when the inversion symmetry is broken in the crystal.[25,26] Assuming long-range polar distortions of the perovskite lattice, it has been speculated that these band splittings

can drastically impact the recombination rates by limiting direct transitions between the valence and conduction bands. This impact was theoretically estimated by Zheng *et al.* to contribute to a reduction of the recombination rates reaching up to two orders of magnitude.[9] However, the existence of long-range polar distortions of iodide-based perovskite lattices is still debated, the influence of Rashba-like spinor band splittings could be more subtle and rather related to local lattice distortions. Moreover, very recent works[27,28] question the role of Rashba splitting in $MAPbI_3$ (MA=methylammonium), where the inversion symmetry breaking is associated to the orientation of methylammonium ions. The Rashba effect can influence carrier transport in halide perovskite also by modifying the carrier mobility, due to modified electron-phonon scattering.[29,30]

Etienne *et al.*[31] investigated by DFT-based molecular dynamics the interplay of electronic and nuclear degrees of freedom in the prototype $MAPbI_3$ perovskite and revealed a dynamical Rashba effect. They reported the influence of temperature and found a spatially local Rashba effect with fluctuations at the subpicosecond time scale, that is to say on the scale of the MA cation motion. Although this time scale is much smaller than the carrier lifetimes, apart from directly affecting radiative recombination probabilities, it could influence the kinetic path for electron-hole recombination.[32] It is worth pointing out that this numerical demonstration by Etienne and coworkers was based on $MAPbI_3$ structures preserving centrosymmetry on the average. They noticed that the Rashba splitting can be quenched when reaching room temperature but also when using larger supercells (up to 32 $MAPbI_3$ units, i.e., 3 nanometers cells) representing a higher and more realistic spatial disorder. The effect is still debated,[33] but an experimental evidence of dynamical Rashba splitting in $MAPbI_3$ was recently reported.[34]

The local and dynamical nature of polar distortions may weaken the influence of Rashba-like spinor splittings by comparison to long range and static polar distortions. However the lack of long range correlations between local polar distortions could be compensated by the unusually strong amplitudes of the atomic motions. The strong anharmonicity of the per-

ovskite lattice is a general feature of this new class of semiconductors,[35] that was pointed out experimentally very early by inelastic neutron scattering in the context of inorganic halide perovskites[36] and that shall give rise to at least two characteristic experimental signatures: large and anisotropic Debye-Waller factors in diffraction studies[37,38] and a so-called quasielastic central peak observed either in inelastic neutron or Raman scattering studies simultaneously with highly damped phonons.[39,40] However, the strong perovskite lattice anharmonicity is not expected to affect only zone center polar optical modes, but also acoustic modes or optical modes located at the edges or the Brillouin zone and related to non-polar antiferrodistortions.[35] The previously mentioned experimental signatures (Debye-waller factors, phonon damping and central peaks by inelastic neutron or Raman scattering studies) can hardly be considered as unambiguous experimental proofs of the existence of strongly anharmonic polar fluctuations. Nowadays direct experimental investigations of the dielectric response give useful indications about the influence of lattice polar distortions[41,42] and the importance of the Fröhlich interaction[43] for electron-phonon coupling processes,[44] but do not directly probe the anaharmonicity of polar distortions. Numerical simulations are therefore still useful tools that already allowed showing the presence of anharmonicity features in $CsPbI_3$,[45,46] leading to symmetry breaking minimum structures in the high temperature phases both at the edges and at the center of the Brillouin zone. MD simulations for $CsPbBr_3$ also suggested that the fluctuations in this material are mostly due to head-to head Cs motion and Br face expansion happening on a few hundred femtosecond time scale.[40]

In that sense, large polar fluctuations of the perovskite lattice at the local scale may lead to two main effects: Rashba-like spinor splittings and strongly anharmonic polarons related to the Fröhlich interaction. We focus in the present contribution on the former aspect.

Computational Details

In this study we started from the minimum reference structures obtained in Ref. 45 which were optimized within Density Functional Theory (DFT) using the Perdew-Burke-Erznerhof (PBE) exchange correlation functional letting both the lattice parameters and the atomic positions relax, keeping the cell's angles fixed. These structures are thus slightly orthorhombic (0.6% distortion). The total energy gain due to the polar distortion is smaller with PBE (3.4 meV) than with the Local Density Approximation (LDA), as reported in Ref. 46 with and without SOC and slightly different settings, but with an analogous energy profile.

For these reference structures, geometry optimizations and force calculations were performed with spin-orbit coupling (SOC). Fully relativistic pseudopotentials were used, with the Cs $[5s^2 5p^6 6s^1]$, I $[5s^2 5p^5]$ and Pb $[5d^{10} 6s^2 6p^2]$ electrons treated as valence states. The choice of 14 electrons for Pb and 9 for Cs was previously discussed.[45] PBE pseudopotentials are ultrasoft ones and were used with a wave function energy cutoff of 25 Ry (200 Ry for the charge density). LDA ones were norm conserving and were used with a 70 Ry wave function cutoff energy.

In order to investigate the effect of spatial and dynamical disorder on the Rashba effect, we proceeded with the following two steps:

- as for the study of the spatial domains, we built anti-ferroelectric configurations with 2×1×1 and 1×1×2 supercells; the corresponding band structure were calculated with fully relativistic pseudopotentials with PBE and SOC. The same calculations were made also with LDA and showed qualitatively similar results.
- in order to study the dynamical Rashba effect we analyzed the electronic structure along a Car-Parrinello Molecular Dynamics (CPMD) trajectory obtained in Ref. 47. The band structure calculations of 50 snapshots were performed with the same fully relativistic US pseudopotentials using the PBE xc functional, in coherence with the CPMD calculations from which MD trajectories were taken,[47] which were done using

PBE as well (with the CP2K code).

The molecular dynamics simulation of Ref. 47 was performed at 370 K under NPT-F conditions, which allow volume fluctuations by changing the supercell edges and angles. The temperature was controlled by a Nose-Hoover thermostat with three chains, and the pressure was controlled by the Martyna's barostat.[48] The time constant for both, the thermostat and barostat, was set at 50 fs. The system used for $CsPbI_3$ has 320 atoms (4×4×4 supercells).

Spin textures were calculated by obtaining the expectation value of the spin operators in the three cartesian directions on a single particle Kohn-Sham wave function ($S_i^\alpha = \langle\psi_i|\sigma_\alpha|\psi_i\rangle$, where $\sigma_\alpha, \alpha = 1, 2, 3$ are the three Pauli spin matrices, ψ_i is a two component spinor eigenfunction). The Brillouin zone was sampled with Γ-centered Monkhorst-Pack meshes[49] with subdivisions of 8×8×8 k-points for unit cells, and corresponding sampling when doubling the cell in x or z directions. The molecular dynamics snapshots were sampled with the Γ point only. Band structures and spin textures were computed with the QUANTUM ESPRESSO package.[50]

Results and Discussion

In this article, we aim to analyze the Rashba effect induced by the anharmonic double well and the influence of symmetry breaking that has been evidenced in the cubic phase of $CsPbI_3$.[45,46] In fact it was shown, using the frozen phonon method, that the highly symmetric cubic phase can be distorted to form two lower-symmetry structures with a slightly lower total energy (by a few meV). These two distorted structures, that we will call in the rest of the article A^+ and A^-, have no inversion symmetry and correspond to the two minimum structures of the double well-instability discussed in Ref. 45. They correspond to opposite ferroelectric distortions ($\eta > 0$ and $\eta < 0$) along a soft polar eigenmode of the centrosymmetric $Pm\bar{3}m$ ("S") structure, represented in Figure 1a, along the x-direction. Note that with rotational symmetry similar studies could be done on the two other eigenmodes corre-

sponding to distortions along the two remaining Cartesian axes (y and z given our labeling). The first aim of the study here is to look at the possible formation of "A^+ domains" and "A^- domains", both in space (supercells) and in time (Car-Parrinello molecular dynamics).

Then, we analyze in detail the dynamical Rashba effect induced by the time dynamics of the oscillations between structure A^+ and structure A^- through the highly symmetric structure S ($\eta = 0$).

Spatial disorder

First, the aim is to investigate the influence of spatial A^+/A^- domains in $CsPbI_3$ on its electronic band structure, in particular in terms of Rashba effect. Given that the eigenvector under study mostly corresponds to a distortion along one axis (here we considered the x-axis) we built supercells by doubling the unit cell either in the x direction or in the z direction. These 2×1×1 and 1×1×2 supercells are built putting together 2 unit cells: 1 unit cell in configuration A^+ (or x up), and another one in configuration A^- (or x down). These supercells, representing modulated structures with the smallest possible period, are schematically shown in Figure 1a.

The Rashba splitting obtained at the R point for a unit cell, in the minimum, symmetry-breaking structure is shown in Figure 1, the blue curve in panels (a) and (b). When doubling the cell along z (resp. x), the R point folds onto the S point (resp. T point), using the orthorhombic convention (in the figure we kept the labels of the cubic unit cell) . For this ordered, static reference structure we find energy splittings of 42 meV (57 meV with LDA) and 24 meV (40 meV with LDA) between the Γ point and, respectively, the conduction band minimum and valence band maximum. In order to give an estimate of the Rashba splitting taking into account the effect both in energy and in the k-space, we calculated the commonly used α_R parameter as defined in Ref. 31:

$$\alpha_R^{C,V} = \frac{\Delta E_{C,V}}{2\Delta k_{C,V}} \quad (1)$$

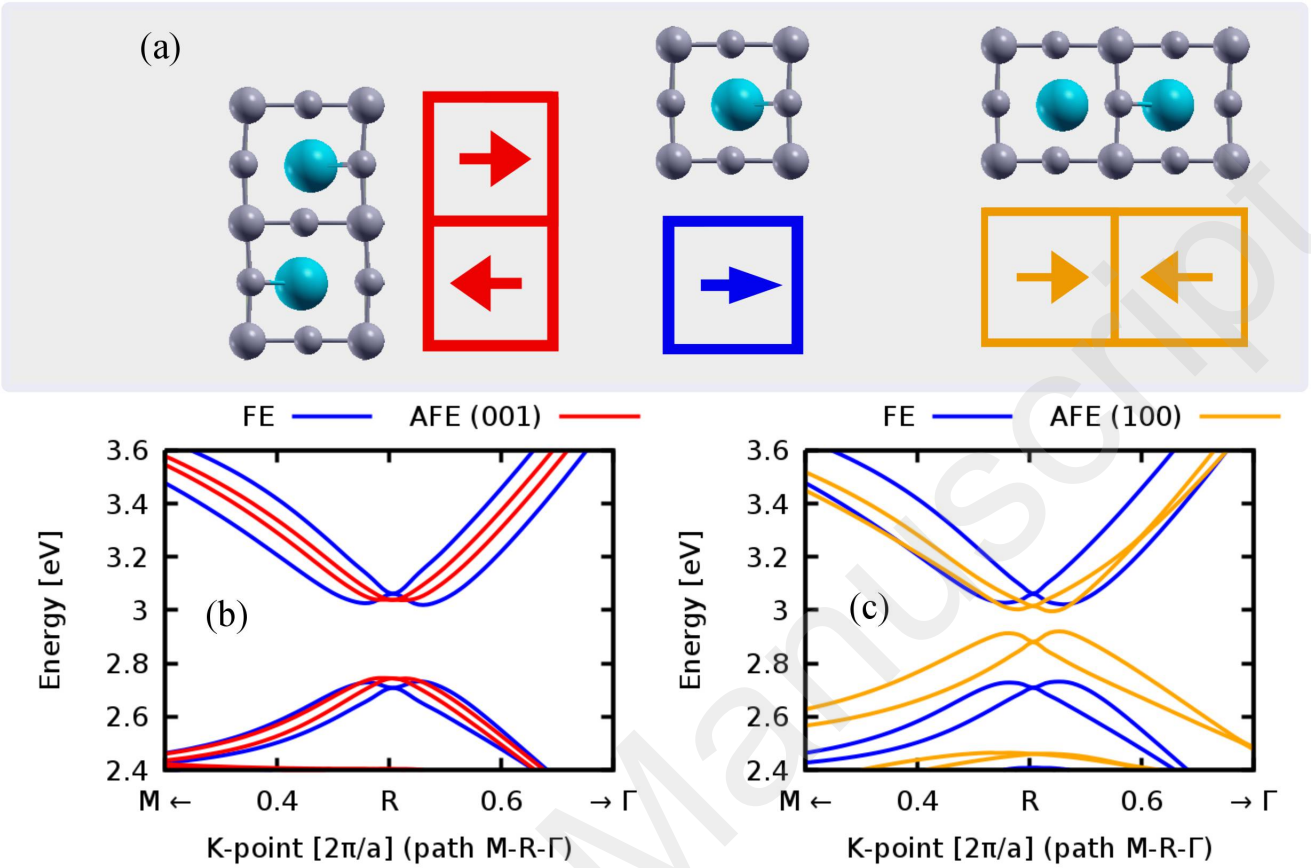

Figure 1: (a) Sketch of the atomic structure and schematic representations of the corresponding unit cells used to study the influence of spatial domains A^+/A^- or "x up"/"x down" on the electronic band structure (arrows represent displacement of Cs, the blue atom). (b,c) Electronic band structure (including SOC) of the 2×1×1 (orange) and 1×1×2 (red) antiferroelectric (AFE) configurations, both compared to the ferroelectric (FE) one (blue). The labelling of the **k**-points is referred to the BZ of the cubic unit cell.

where $\Delta E_{C,V}$ is the energy difference between the first (resp. last) two bands of the conduction (resp. valence) bands and $\Delta k_{C,V}$ the splitting of the minimum (resp. maximum) in k-space. For the reference, static, highly ordered structure we found α_R values of 3.04 (4.09 with LDA) eV·Å and 2.75 (2.01 with LDA) eV·Å for the conduction and the valence bands, respectively. These values are comparable to those reported in Ref. 31 in the case of polar $MAPbI_3$: 3.17 eV·Å and 1.17 eV·Å respectively. Note that so far the highest values found in ferroelectric materials for the Rashba parameter are 4.2-4.8 eV·Å for GeTe.[51,52]

The results for the two modulated structures are shown in Figures 1b and 1c. Whereas no

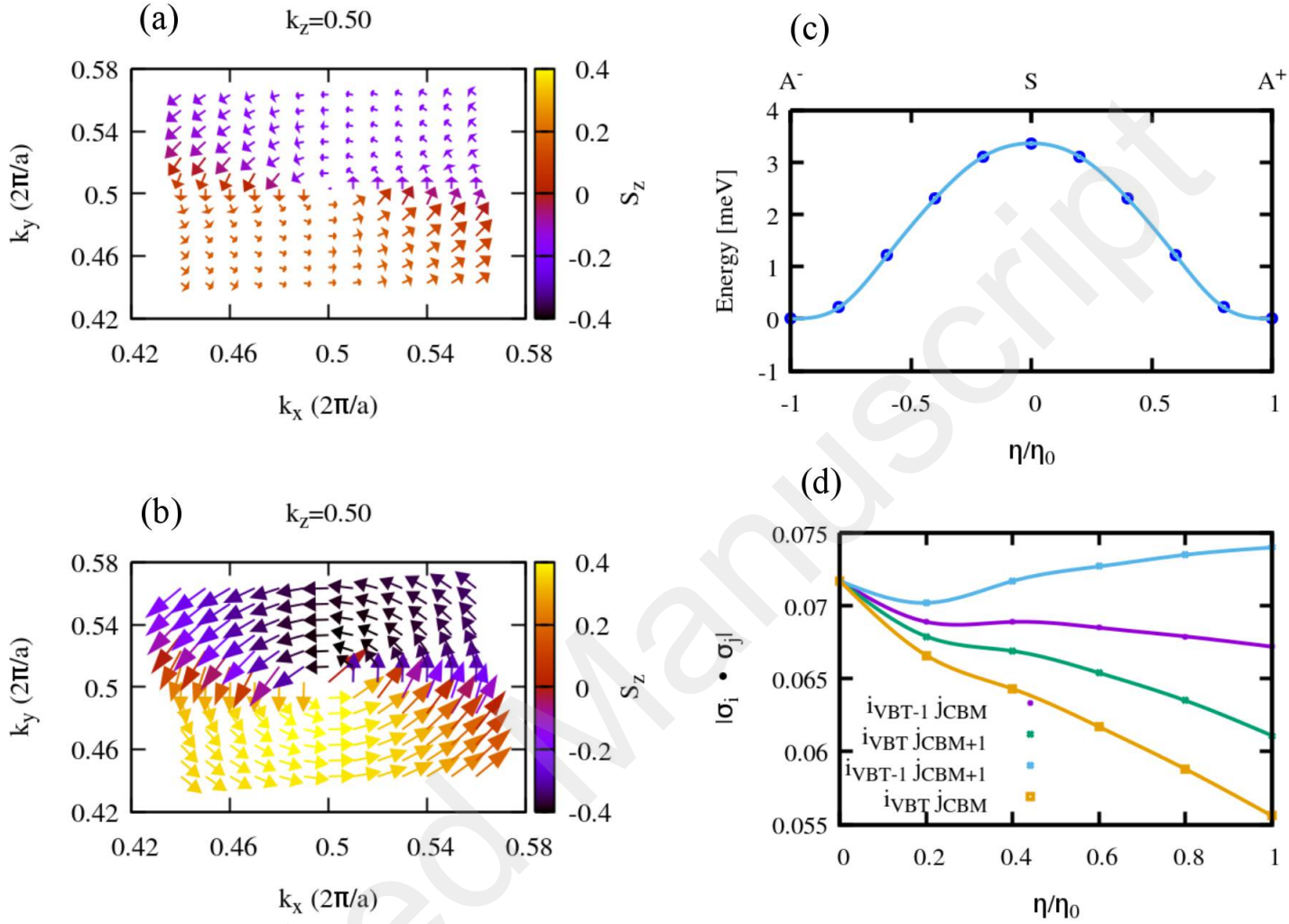

Figure 2: Spin textures for the last occupied valence band (a) and the first empty conduction one (b) in a cube with side $0.12\times\frac{2\pi}{a}$ surrounding the R point of the BZ, for the asymmetric A^+ configuration. A section with k_z=$0.5\times\frac{2\pi}{a}$ is shown. The third panel (c) shows the energy profile of the double well between the A^-, S and A^+ configurations and panel (d) shows the integral of four scalar products between the spin vector expectation values of a valence and a conduction state as a function of the polar distortion leading from the centrosymmetric ($Pm\bar{3}m$) S structure ($\eta/\eta_0 = 0$) to the distorted minimum energy A^+ structure ($\eta/\eta_0 = 1$), where the inversion symmetry is broken. The last two occupied states (VBT-1 and VBT) and the first two empty ones (CBM and CBM+1) are considered.

Rashba effect is found in the case of a modulation orthogonal to the direction of symmetry breaking, a band splitting around the valence band maximum and the conduction band minimum is found for a modulation parallel to the direction of symmetry breaking. We

found α_R values of 1.98 (0.58 with LDA) eV·$\AA$ and 2.97 (2.18 with LDA) eV·$\AA$ for the conduction and valence bands, respectively.

In general, the Rashba splitting in the band structure of a two-dimensional system results from the combined effect of atomic spin-orbit coupling and asymmetry of the potential in the direction (here x) perpendicular to the two-dimensional plane, causing a loss of inversion symmetry. In the case of a modulation orthogonal to the direction of symmetry breaking (1×1×2 supercell), the symmetry along x is respected on average: the inversion symmetry is kept and the Rashba splitting vanishes. We expect then that the quenching of the Rashba effect results from a competition between parallel and orthogonal modulations: the former keeps the Rashba effect, while the latter tends to cancel it.

According to Rashba model hamiltonians the spin texture is such that the top of the valence band and bottom of the conduction band of the splitted bands have opposite spin orientations, reducing thus the recombination probability at the band gap. It has been recently shown, through full ab initio calculation of the spin texture,[27] that this picture is not realistic for $MAPbI_3$, because the spin mismatch between the highest valence band and the lowest conduction bands is small and, as such, not expected to reduce the recombination rate in a significant way. In $MAPbI_3$ inversion symmetry is broken by a combination of orientation of the methylammonium molecular ion and the distortion it induces in the inorganic network. It is then difficult to disentangle the two effects. $CsPbI_3$ is a useful playground to single out the effect of the polar distortion. Calculating the spin texture in a region of the BZ close to the R point of the cubic structure we found that, as for $MAPbI_3$, the spin orientations are similar around the R point for the last occupied and the first empty states. We show two maps in panels (a) and (b) of Figure 2. They refer to the broken symmetry configuration A^+ (the energy profile of the double well is reminded in figure 2c). In order to quantitatively assess the collinearity of the spins of valence and conduction states close to the band gap, as a function of the polar distortion, we show, in panel (d) of Figure 2, the integral of the modulus of the scalar product of valence/conduction spin vectors in a cube of size $0.12\times\frac{2\pi}{a}$

around the R-point; the four possible combinations between the last two valence bands and the first two conduction ones are presented. The curves show that all the four products have similar order of magnitudes, that the lowest value is the one between the last occupied band and the first empty one and, finally, that the polar distortion does indeed enhance the spin mismatch of three out of four valence/conduction pairs.

Dynamical structural fluctuations

Next, we analyze in detail CPMD trajectories of cubic $CsPbI_3$ in the light of our findings on the double well potential energy surface. The trajectories were computed by Carignano *et al.* in the framework of a study[47] of the anharmonic motion of the iodine atoms in $CsPbI_3$ and $MAPbI_3$, where they showed that, at variance with $FAPbI_3$, these two perovskite structures are expected to have a deviation from the perfect cubic unit cell at any time of the MD, with a probability very close to 1. This hints towards the interpretation that the $Pm\bar{3}m$ symmetry can be seen as a time average, including for $CsPbI_3$. This phenomenon had already been reported for $MAPbI_3$ in earlier studies,[18] where it was evidenced that the system strongly deviates from the perfectly cubic structure in the sub-picosecond time scale.

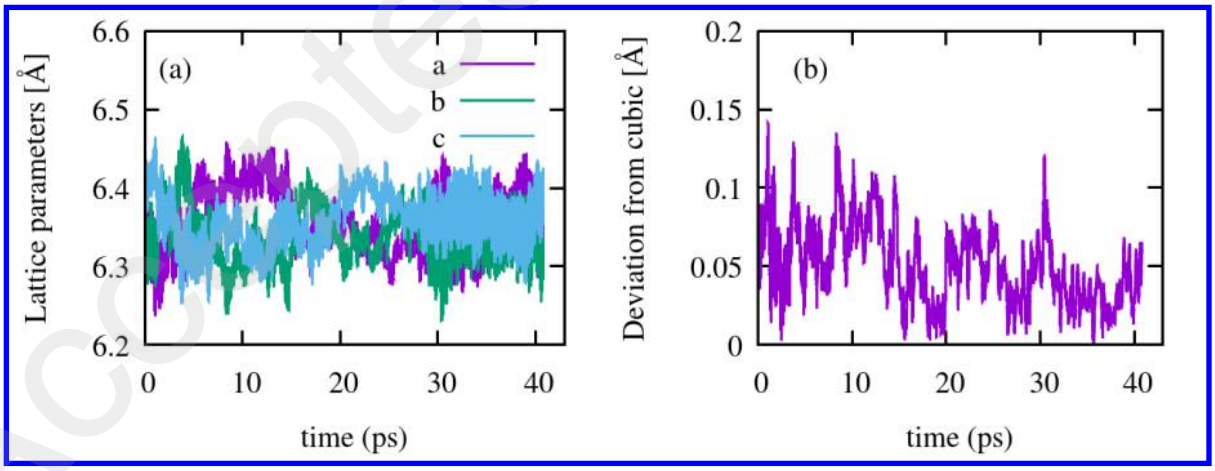

Figure 3: (a) Lattice parameters fluctuations along the CPMD trajectory at 370 K. (b) Fluctuations of the deviation from the average pseudocubic structure, as defined in Eq. 2.

In Figures 3a we show the lattice parameters fluctuations versus time. In particular, from

this first simple analysis we can infer that the structure fluctuates around a cubic structure: the difference between the lattice parameters stays below 3%. Even though the structure is not perfectly cubic on average (see Table 1), the deviation from the average pseudocubic lattice structure (Figure 3b) is smaller than 1%. This deviation d is a cartesian distance obtained as:

$$d(t) = \sqrt{\sum_{i=1}^{3} (x_i(t) - \bar{x_i})^2} \quad (2)$$

where x_i are the three lattice parameters and $\bar{x_i}$ their time average over the whole trajectory.

Table 1: Average lattice parameters (in Angstroms) along the CPMD trajectories at 370 K and 450 K.

In Angstroms	370 K	450 K
a	6.358	6.372
b	6.338	6.391
c	6.358	6.361

In order to analyze the MD trajectories in the light of the aforementioned double well instability, we project these trajectories onto two kind of structures: the perfectly cubic symmetric structure ("S") and the symmetry breaking structures A^+ and A^-. The chosen approach is to study the radial distribution function of the cesium-lead pairs during the MD simulation and to compare it to our two reference structures.

Figure 4 focuses on averages over 0.5 ps intervals. At this time scale, our double well references seem to explain very well how the system explores the energy landscape. Whereas some intervals show a distance peak corresponding to the distance in the average pseudocubic structure S, others, for instance the [11-11.5 ps] interval, show two peaks centered on both minimum structures A^+ and A^-. This means that within 0.5 ps the structure has enough time to explore the whole double well. We think that this is the most appropriate time-scale to evidence the double well instabilities.

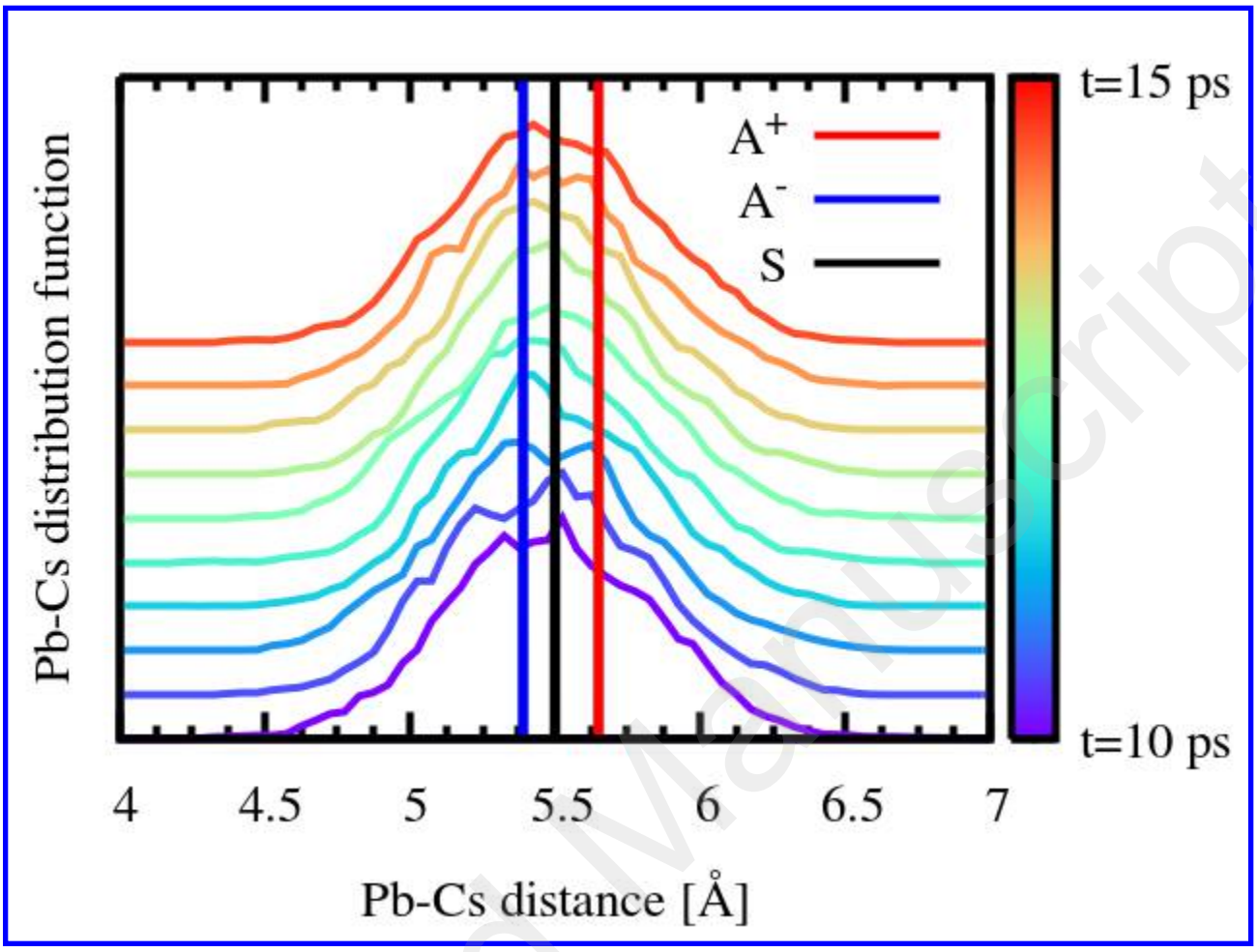

Figure 4: Distribution function of the cesium-lead pairs' distances along the MD trajectory. Here the references (vertical lines) correspond to the distances for structures S, A^+ and A^-, weighted by the ratio between the lattice parameters.

Dynamical Rashba effect

We now focus on the dynamical Rashba effect possibly ensuing from the nuclear dynamics exposed above. We expect to find in $CsPbI_3$ an effect similar to what was evidenced for $MAPbI_3$ for which the spatially local Rashba splitting was found to fluctuate on the subpicosecond time scale typical of the methylammonium cation dynamics.[31]

To investigate this effect, we calculate the electronic band structure, including spin-orbit coupling, at different snapshots along the trajectory. Given the results of the Pb-Cs distance analysis, we chose to focus these calculations on the [10-15 ps] interval in which we chose 50

regularly distributed snapshots (hence separated by 100 fs from each other) in order to better capture the sub pico-second dynamics. For each snapshot, we used the MD structure of the 4×4×4 supercells (we remind the reader that the cell's atomic positions, lattice parameters and angles vary) and derived its electronic band structure. These calculations for 4×4×4 supercells follow the guidelines of those previously done for $MAPbI_3$.[18]

The electronic band structure calculations are performed for 7 **k** points of the Brillouin zone and, from these, parabolic bands in the vicinity of the Γ point were obtained (see the Supporting Information for further details). In Figure 5 we plot, for each snapshot i of the 50 structures chosen in the MD trajectory and for each **k** point, the normalized energy difference defined as:

$$\Delta E^i_{gap}(k) = [CBM^i(k) - VBT^i(k)] - [(CBM^i(\Gamma) - VBT^i(\Gamma))] \quad (3)$$

where CBM is the conduction band minimum and VBT the valence band top. This is necessary as the cell is variable along the trajectory: the fluctuations on the gap value, which are large with respect to the Rashba splitting, would mask it otherwise. The corresponding plots for the valence and conduction bands as well as the evolution of the bandgap over time are presented in the supporting information.

These results show that 100 fs is a good estimate of the timescale of the Rashba effect dynamics. Moreover, on average we see a band gap shift towards the y direction, the band gap being reduced by 1.3 meV on average. Taking the extreme case, we can infer that the amplitude of the oscillations in the 5 ps timescale is around 10 meV. Further analysis of the time coherence of the Rashba effect are provided in the supporting information file through time correlation functions.

Figure S1 shows that this is mostly due to a Rashba splitting happening at the CBM rather than at the VBT. This is coherent with the fact that the most relativistic atom, Pb, is mostly contributing to the conduction band and with what was previously reported for $MAPbI_3$[18] as well.

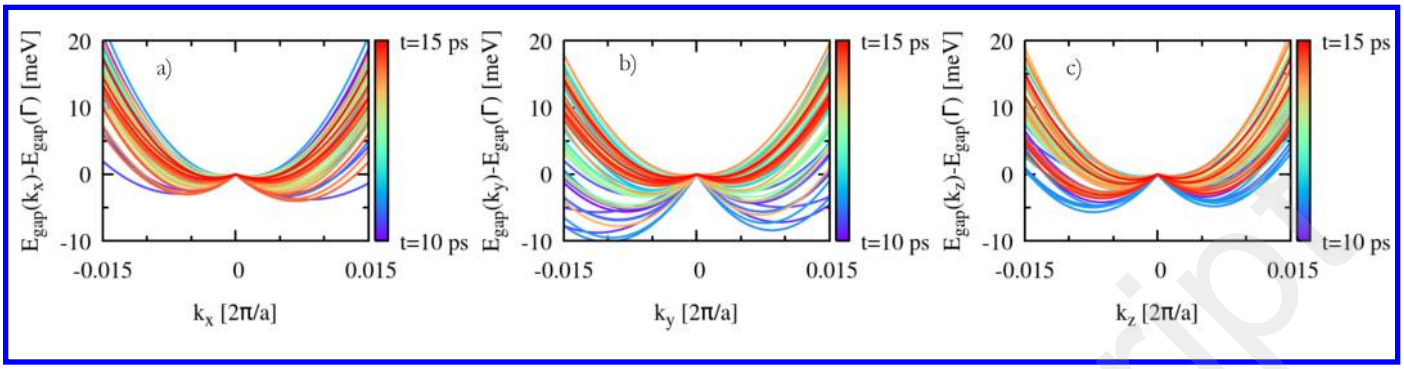

Figure 5: Differences between the gap at finite **k** and at Γ for the 50 snapshots chosen along the MD trajectory. The three panels a-c refer to the three directions, $\mathbf{k}_x$, $\mathbf{k}_x$ $\mathbf{k}_z$. This difference is 0 at Γ by construction (see Eq. 3).

Figure 6a represents the oscillations of the Rashba effect in this interval through the previously defined α_R parameter. This result confirms that the Rashba effect is much more substantial for the conduction band than for the valence band, and oscillates with values close to 1 eV·Å. Even though this is smaller than in the static case (values around 3 eV·Å), this means that the effect is still sizable despite the disorder induced by temperature and the large investigated supercell.

It is interesting to further look into these oscillations through a Fourier analysis (Figure 6b) which reveals the existence of two main frequency components :

- A 2.5 ps component (frequency: 0.4 THz or 13 cm^{-}1), compatible with the back and forth jump through the double well and thus to the slow motion of the Cs cation;
- A 0.8 ps component (frequency: 1.2 THz or 40 cm^{-}1) corresponding to the phonon modes usually associated to the Pb-I stretching (around 20-40 cm^{-1}).

We further compare the order of magnitudes of these oscillations to those obtained in a similar study lead on hybrid perovskite $MAPbI_3$ by Etienne *et al.*.[31] We report in Table 2 the corresponding values for the apolar structure of Ref. 31, because a Cs atom has no permanent dipole moment. Note that nevertheless, for the polar structure, the largest α_R value reported in Ref. 31 (10.36 eV·Å) is even smaller than the largest one reported for the non-polar

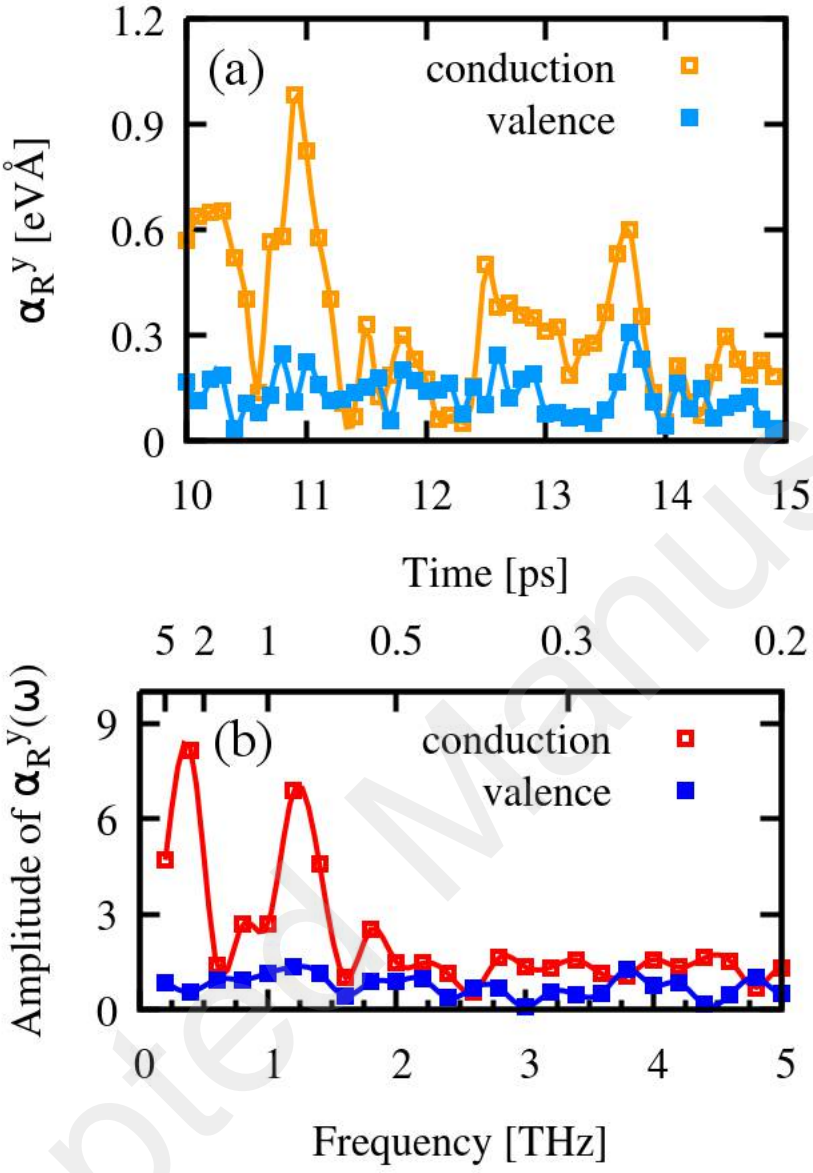

Figure 6: (a) α_R parameter for the conduction and valence bands (in the $\mathbf{k}_y$ direction) versus time. (b) Fourier transform of the Rashba parameter α_R shown in panel (a).

structure. One needs to keep in mind that we have here very large supercells compared to what was used in that study. The conclusion we can draw from this comparison is that we observe a sizable dynamical Rashba effect even with large supercells and in the absence of the organic molecule, which in general is a possible source of symmetry breaking in these halide perovskite structures. The fact that the order of magnitude of the dynamical Rashba

splitting is similar for $MAPbI_3$ and $CsPbI_3$ is in agreement with the recent observation of similar recombination kinetics for both compounds.[53]

Table 2: Maximum value of the α_R oscillations.

Number of formula units	α_R for hybrid $MAPbI_3$ from Ref. 31 (eV.Å)	α_R for inorganic $CsPbI_3$ from our results (eV.Å)
1	12.48	
4	3.86	
32	2.19	
64		0.96

Concluding remarks

In summary, we investigated the effect of spatial and temporal disorder on the Rashba splitting in the cubic α-phase of inorganic halide perovskite $CsPbI_3$. The analysis focused on the fluctuations of the Rashba parameter α_R —a measure of the Rashba band splitting— along a molecular dynamics trajectory for a large supercell.[47] Our results highlight a dynamical Rashba effect similar to the one previously observed for hybrid organic-inorganic halide perovskites,[31] which persists in spite of the quenching effect coming from spatial disorder in this relatively large simulation cell (320 atoms). Some low-frequency vibrational modes of the system, and in particular the anharmonic behavior, which has been shown to originate from the double well potential energy landscape of a polar optical phonon,[45] contribute to the spatial extension of the Rashba effect. This is confirmed by the Fourier analysis of the fluctuations of the Rashba parameter α_R.

An expected consequence of the Rashba effect is the reduction of the carriers recombination rate[9] and consequent enhancement of their radiative lifetime; however, this effect is submitted to a specific spin texture which has been recently shown not to occur in $MAPbI_3$. Our calculated ab initio spin textures in $CsPbI_3$ suggest that, although a reduction of the recombination rate due to Rashba splitting is indeed expected, its effect is not as large as

previous model calculations had predicted.

Supporting Information Available

We provide in the supporting information additional results on the effect of dynamical disorder on the conduction band minimum and valence band top throughout the chosen 5 ps interval of study for our band structure calculations. We also provide an analysis of the time correlation of the Rashba parameter α (or α_R) and of the spin textures.

Acknowledgement

Dr. Arthur Marronnier's PhD project was funded by the Graduate School of École des Ponts ParisTech and the French Department of Energy (MTES). HPC resources of TGCC and CINES were used through allocation 2017090642 and x20170906724 GENCI projects. The work at FOTON and ISCR was funded by the European Union's Horizon 2020 program, through a FET Open research and innovation action under the grant agreement No 687008.

References

(1) Sanehira, E. M.; Marshall, A. R.; Christians, J. A.; Harvey, S. P.; Ciesielski, P. N.; Wheeler, L. M.; Schulz, P.; Lin, L. Y.; Beard, M. C.; Luther, J. M. Enhanced Mobility $CsPbI_3$ Quantum Dot Arrays for Record-efficiency, High-voltage Photovoltaic Cells. *Sci. Adv.* **2017**, *3*, eaaao4204.

(2) Wang, K.; Jin, Z.; Liang, L.; Bian, H.; Bai, D.; Wang, H.; Zhang, J.; Wang, Q.; Shengzhong, L. All-inorganic Cesium Lead Iodide Perovskite Solar Cells with Stabilized Efficiency Beyond 15% . *Nat. Commun.* **2018**, *9*, 4544.

(3) Saliba, M.; Matsui, T.; Seo, J.-Y.; Domanski, K.; Correa-Baena, J.-P.; Nazeerud-

din, M. K.; Zakeeruddin, S. M.; Tress, W.; Abate, A.; Hagfeldt, A. et al. Cesium-containing Triple Cation Perovskite Solar Cells: Improved Stability, Reproducibility and High Efficiency. *Energy Environ. Sci.* **2016**, *9*, 1989–1997.

(4) Chiarella, F.; Zappettini, A.; Licci, F.; Borriello, I.; Cantele, G.; Ninno, D.; Cassinese, A.; Vaglio, R. Combined Experimental and Theoretical Investigation of Optical, Structural, and Electronic Properties of $CH_3NH_3SnX_3$ Thin Films (X= Cl, Br). *Phys. Rev. B* **2008**, *77*, 045129.

(5) Ogomi, Y.; Morita, A.; Tsukamoto, S.; Saitho, T.; Fujikawa, N.; Shen, Q.; Toyoda, T.; Yoshino, K.; Pandey, S. S.; Ma, T. et al. $CH_3NH_3Sn_xPb_{(1-x)}I_3$ Perovskite Solar Cells Covering up to 1060 nm. *J. Phys. Chem. Lett.* **2014**, *5*, 1004–1011.

(6) Eperon, G. E.; Stranks, S. D.; Menelaou, C.; Johnston, M. B.; Herz, L. M.; Snaith, H. J. Formamidinium Lead Trihalide: a Broadly Tunable Perovskite for Efficient Planar Heterojunction Solar Cells. *Energy Environ. Sci.* **2014**, *7*, 982–988.

(7) Stoumpos, C. C.; Malliakas, C. D.; Kanatzidis, M. G. Semiconducting Tin and Lead Iodide Perovskites with Organic Cations: Phase Transitions, High Mobilities, and Near-Infrared Photoluminescent Properties. *Inorg. Chem.* **2013**, *52*, 9019–9038.

(8) Wehrenfennig, C.; Liu, M.; Snaith, H. J.; Johnston, M. B.; Herz, L. M. Charge-carrier Dynamics in Vapour-deposited Films of the Organolead Halide Perovskite CH_3 NH_3 PbI_{3-x} Cl_x. *Energy Environ. Sci.* **2014**, *7*, 2269–2275.

(9) Zheng, F.; Tan, L. Z.; Liu, S.; Rappe, A. M. Rashba Spin–orbit Coupling Enhanced Carrier Lifetime in $CH_3NH_3PbI_3$. *Nano Lett.* **2015**, *15*, 7794–7800.

(10) Ponseca Jr, C. S.; Savenije, T. J.; Abdellah, M.; Zheng, K.; Yartsev, A.; Pascher, T.; Harlang, T.; Chabera, P.; Pullerits, T.; Stepanov, A. et al. Organometal Halide Perovskite Solar Cell Materials Rationalized: Ultrafast Charge Generation, High and

Microsecond-long Balanced Mobilities, and Slow Recombination. *J. Am. Chem. Soc.* **2014**, *136*, 5189–5192.

(11) Cahen, D.; Edri, E.; Hodes, G.; Gartsman, K.; Kirmayer, S.; Mukhopadhyay, S. Elucidating the Charge Carrier Separation and Working Mechanism of CH_3 NH_3 PbI_{3-x} Cl_x Perovskite Solar Cells. *Nat. Commun.* **2014**, *5*, 3461.

(12) Xing, G.; Mathews, N.; Sun, S.; Lim, S. S.; Lam, Y. M.; Grätzel, M.; Mhaisalkar, S.; Sum, T. C. Long-range Balanced Electron-and Hole-transport Lengths in Organic-inorganic $CH_3NH_3PbI_3$. *Science* **2013**, *342*, 344–347.

(13) Stranks, S. D.; Eperon, G. E.; Grancini, G.; Menelaou, C.; Alcocer, M. J.; Leijtens, T.; Herz, L. M.; Petrozza, A.; Snaith, H. J. Electron-hole Diffusion Lengths Exceeding 1 micrometer in an Organometal Trihalide Perovskite Absorber. *Science* **2013**, *342*, 341–344.

(14) Lee, H.; Gaiaschi, S.; Chapon, P.; Marronnier, A.; Lee, H.; Vanel, J.-C.; Tondelier, D.; Boureé, J.-E.; Bonnassieux, Y.; Geffroy, B. Direct Experimental Evidence of Halide Ionic Migration under Bias in $CH_3NH_3PbI_{3-x}Cl_x$-Based Perovskite Solar Cells Using GD-OES Analysis. *ACS Energy Lett.* **2017**, *2*, 943–949.

(15) Yang, T.-Y.; Gregori, G.; Pellet, N.; Grätzel, M.; Maier, J. The Significance of Ion Conduction in a Hybrid Organic–inorganic Lead-iodide-based Perovskite Photosensitizer. *Angew. Chem., Int. Ed.* **2015**, *127*, 8016–8021.

(16) Even, J.; Pedesseau, L.; Katan, C. Analysis of Multivalley and Multibandgap Absorption and Enhancement of Free Carriers Related to Exciton Screening in Hybrid Perovskites. *J. Phys. Chem. C* **2014**, *118*, 11566–11572.

(17) Ma, J.; Wang, L.-W. Nanoscale Charge Localization Induced by Random Orientations of Organic Molecules in Hybrid Perovskite $CH_3NH_3PbI_3$. *Nano Lett.* **2014**, *15*, 248–253.

(18) Quarti, C.; Mosconi, E.; Ball, J. M.; D'Innocenzo, V.; Tao, C.; Pathak, S.; Snaith, H. J.; Petrozza, A.; De Angelis, F. Structural and Optical Properties of Methylammonium Lead Iodide across the Tetragonal to Cubic Phase Transition: Implications for Perovskite Solar Cells. *Energy Environ. Sci.* **2016**, *9*, 155–163.

(19) Davies, C. L.; Filip, M. R.; Patel, J. B.; Crothers, T. W.; Verdi, C.; Wright, A. D.; Milot, R. L.; Giustino, F.; Johnston, M. B.; Herz, L. M. Bimolecular Recombination in Methylammonium Lead Triiodide Perovskite is an Inverse Absorption Process. *Nat. Commun.* **2018**, *9*, 293.

(20) Even, J.; Pedesseau, L.; Jancu, J.-M.; Katan, C. Importance of Spin–orbit Coupling in Hybrid Organic/Inorganic Perovskites for Photovoltaic Applications. *J. Phys. Chem. Lett.* **2013**, *4*, 2999–3005.

(21) Kim, M.; Im, J.; Freeman, A. J.; Ihm, J.; Jin, H. Switchable $S = 1/2$ and $J = 1/2$ Rashba Bands in Ferroelectric Halide Perovskites. *Proc. Natl. Acad. Sci. U. S. A.* **2014**, *111*, 6900–6904.

(22) Even, J.; Pedesseau, L.; Jancu, J.-M.; Katan, C. DFT and $\mathbf{k} \cdot \mathbf{p}$ Modelling of the Phase Transitions of Lead and Tin Halide Perovskites for Photovoltaic Cells. *Phys. Status Solidi RRL* **2014**, *8*, 31–35.

(23) Amat, A.; Mosconi, E.; Ronca, E.; Quarti, C.; Umari, P.; Nazeeruddin, M. K.; Grätzel, M.; De Angelis, F. Cation-Induced Band-Gap Tuning in Organohalide Perovskites: Interplay of Spin–Orbit Coupling and Octahedra Tilting. *Nano Lett.* **2014**, *14*, 3608–3616.

(24) Brivio, F.; Butler, K. T.; Walsh, A.; van Schilfgaarde, M. Relativistic Quasiparticle Self-consistent Electronic Structure of Hybrid Halide Perovskite Photovoltaic Absorbers. *Phys. Rev. B* **2014**, *89*, 155204.

(25) Zhang, X.; Liu, Q.; Luo, J.-W.; Freeman, A. J.; Zunger, A. Hidden Spin Polarization in Inversion-symmetric Bulk Crystals. *Nat. Phys.* **2014**, *10*, 387.

(26) Kepenekian, M.; Robles, R.; Katan, C.; Sapori, D.; Pedesseau, L.; Even, J. Rashba and Dresselhaus Effects in Hybrid Organic–Inorganic Perovskites: From Basics to Devices. *ACS Nano* **2015**, *9*, 11557–11567.

(27) Zhang, X.; Shen, J.-X.; Van de Walle, C. G. Three-Dimensional Spin Texture in Hybrid Perovskites and Its Impact on Optical Transitions. *J. Phys. Chem. Lett.* **2018**, *9*, 2903–2908.

(28) Zhang, X.; Shen, J.-X.; Wang, W.; Van de Walle, C. G. First-Principles Analysis of Radiative Recombination in Lead-Halide Perovskites. *ACS Energy Lett.* **2018**, *3*, 2329–2334.

(29) Yu, Z.-G. Rashba Effect and Carrier Mobility in Hybrid Organic-Inorganic Perovskites. *J. Phys. Chem. Lett.* **2016**, *7*, 3078–3083.

(30) Kang, Y.; Han, S. Intrinsic Carrier Mobility of Cesium Lead Halide Perovskites. *Phys. Rev. Appl.* **2018**, *10*, 044013.

(31) Etienne, T.; Mosconi, E.; De Angelis, F. Dynamical Origin of the Rashba Effect in Organohalide Lead Perovskites: A Key to Suppressed Carrier Recombination in Perovskite Solar Cells? *J. Phys. Chem. Lett.* **2016**, *7*, 1638–1645.

(32) Hutter, E. M.; Savenjie, T. J. Thermally Activated Second-Order Recombination Hints toward Indirect Recombination in Fully Inorganic $CsPbI_3$ Perovskites. *ACS Energy Lett.* **2018**, *3*, 2068–2069.

(33) Frohna, K.; Deshpande, T.; Harter, J.; Peng, W.; Barker, B. A.; Neaton, J. B.; Louie, S. G.; Bakr, O. M.; Hsieh, D.; Bernardi, M. Inversion Symmetry and Bulk

Rashba Effect in Methylammonium Lead Iodide Perovskite Single Crystals. *Nat. Commun.* **2018**, *9*, 1829.

(34) Niesner, D.; Hauck, M.; Shrestha, S.; Levchuk, I.; Matt, G. J.; Osvet, A.; Batentschuk, M.; Brabec, C.; Weber, H. B.; Fauster, T. Structural Fluctuations Cause Spin-split States in Tetragonal $(CH_3NH_3)PbI_3$ as Evidenced by the Circular Photogalvanic Effect. *Proc. Natl. Acad. Sci. U. S. A.* **2018**, *115*, 9509–9514.

(35) Katan, C.; Mohite, A. D.; Even, J. Riddles in Perovskite Research. *Nat. Mater.* **2018**, *17*, 377–384.

(36) Fujii, Y.; Hoshino, S.; Yamada, Y.; Shirane, G. Neutron-scattering Study on Phase Transitions of $CsPbCl_3$. *Phys. Rev. B* **1974**, *9*, 4549–4559.

(37) Trots, D.; Myagkota, S. High-temperature Structural Evolution of Caesium and Rubidium Triiodoplumbates. *J. Phys. Chem. Solids* **2008**, *69*, 2520–2526.

(38) Hutton, J.; Nelmes, R.; Meyer, G.; Eiriksson, V. High-resolution Studies of Cubic Perovskites by Elastic Neutron Diffraction: $CsPbCl_3$. *J. Phys. C: Solid State Phys.* **1979**, *12*, 5393.

(39) Even, J.; Carignano, M.; Katan, C. Molecular Disorder and Translation/Rotation Coupling in the Plastic Crystal Phase of Hybrid Perovskites. *Nanoscale* **2016**, *8*, 6222–6236.

(40) Yaffe, O.; Guo, Y.; Tan, L. Z.; Egger, D. A.; Hull, T.; Stoumpos, C. C.; Zheng, F.; Heinz, T. F.; Kronik, L.; Kanatzidis, M. G. et al. Local Polar Fluctuations in Lead Halide Perovskite Crystals. *Phys. Rev. Lett.* **2017**, *118*, 136001.

(41) Marronnier, A.; Lee, H.; Lee, H.; Kim, M.; Eypert, C.; Gaston, J.-P.; Roma, G.; Tondelier, D.; Geffroy, B.; Bonnassieux, Y. Electrical and Optical Degradation Study of Methylammonium-based Perovskite Materials under Ambient Conditions. *Sol. Energy Mater. Sol. Cells* **2018**, *178*, 179–185.

(42) Anusca, I.; Balčiūnas, S.; Gemeiner, P.; Svirskas, Š.; Sanlialp, M.; Lackner, G.; Fettkenhauer, C.; Belovickis, J.; Samulionis, V.; Ivanov, M. et al. Dielectric response: Answer to Many Questions in the Methylammonium Lead Halide Solar Cell Absorbers. *Adv. Energy Mater.* **2017**, *7*, 1700600.

(43) Sendner, M.; Nayak, P. K.; Egger, D. A.; Beck, S.; Müller, C.; Epding, B.; Kowalsky, W.; Kronik, L.; Snaith, H. J.; Pucci, A. et al. Optical Phonons in Methylammonium Lead Halide Perovskites and Implications for Charge Transport. *Mater. Horiz.* **2016**, *3*, 613–620.

(44) Fu, M.; Tamarat, P.; Trebbia, J.-B.; Bodnarchuk, M. I.; Kovalenko, M. V.; Even, J.; Lounis, B. Unraveling Exciton–phonon Coupling in Individual $FAPbI_3$ Nanocrystals Emitting Near-infrared Single Photons. *Nat. Commun.* **2018**, *9*, 3318.

(45) Marronnier, A.; Lee, H.; Geffroy, B.; Even, J.; Bonnassieux, Y.; Roma, G. Structural Instabilities Related to Highly Anharmonic Phonons in Halide Perovskites. *J. Phys. Chem. Lett.* **2017**, *8*, 2659–2665.

(46) Marronnier, A.; Roma, G.; Boyer-Richard, S.; Pedesseau, L.; Jancu, J.-M.; Bonnassieux, Y.; Katan, C.; Stoumpos, C. C.; Kanatzidis, M. G.; Even, J. Anharmonicity and Disorder in the Black Phases of Cesium Lead Iodide Used for Stable Inorganic Perovskite Solar Cells. *ACS Nano* **2018**, *12*, 3477–3486.

(47) Carignano, M. A.; Aravindh, S. A.; Roqan, I. S.; Even, J.; Katan, C. Critical Fluctuations and Anharmonicity in Lead Iodide Perovskites from Molecular Dynamics Supercell Simulations. *J. Phys. Chem. C* **2017**, *121*, 20729–20738.

(48) Martyna, G. J.; Tuckerman, M. E.; Tobias, D. J.; Klein, M. L. Explicit Reversible Integrators for Extended Systems Dynamics. *Mol. Phys.* **1996**, *87*, 1117–1157.

(49) Monkhorst, H. J.; Pack, J. D. Special points for Brillouin-zone integrations. *Phys. Rev. B* **1976**, *13*, 5188–5192.

(50) Giannozzi, P.; Baroni, S.; Bonini, N.; Calandra, M.; Car, R.; Cavazzoni, C.; Ceresoli, D.; Chiarotti, G. L.; Cococcioni, M.; Dabo, I. et al. Quantum Espresso: a Modular and Open-source Software Project for Quantum Simulations of Materials. *J. Phys.: Condens. Matter* **2009**, *21*, 395502.

(51) Picozzi, S. Ferroelectric Rashba Semiconductors as a Novel Class of Multifunctional Materials. *Front. Condens. Matter Phys. Res.* **2014**, *2*, 10.

(52) Krempaský, J.; Volfová, H.; Muff, S.; Pilet, N.; Landolt, G.; Radović, M.; Shi, M.; Kriegner, D.; Holý, V.; Braun, J. et al. Disentangling Bulk and Surface Rashba Effects in Ferroelectric α-GeTe. *Phys. Rev. B* **2016**, *94*, 205111.

(53) Dastidar, S.; Li, S.; Smolin, S. Y.; Baxter, J. B.; Fafarman, A. T. Slow Electron-Hole Recombination in Lead Iodide Perovskites Does Not Require a Molecular Dipole. *ACS Energy Lett.* **2017**, *2*, 2239–2244.

TOC Graphic